IEICE TRANS. COMMUN., VOL.E87–B, NO.11 NOVEMBER 2004

PAPER

A Phase Compensation Algorithm for High-Resolution Pulse Radar Systems

Takuya SAKAMOTO[†a)], ***Student Member and*** **Toru SATO**[†], ***Member***

SUMMARY Imaging techniques for robots are important and meaningful in the near future. Pulse radar systems have a great potential for shape estimation and locationing of targets. They have an advantage that they can be used even in critical situations where optical techniques cannot be used. It is thus required to develop high-resolution imaging algorithms for pulse radar systems. High-resolution imaging algorithms utilize the carrier phase of received signals. However, their estimation accuracy suffers degradation due to phase rotation of the received signal because the phase depends on the shape of the target. In this paper, we propose a phase compensation algorithm for high-resolution pulse radar systems. The proposed algorithm works well with SEABED algorithm, which is a non-parametric algorithm of estimating target shapes based on a reversible transform. The theory is presented first and numerical simulation results follow. We show the estimation accuracy is remarkably improved without sacrificing the resolution using the proposed algorithm.

key words: *pulse radar, phase compensation, shape estimation, ill-posed inverse problem, boundary scattering transform*

1. Introduction

It is expected that rescue robots will autonomously wander indoors and outdoors in the near future. They require locationing techniques for their autonomous operation. Shape estimation of nearby objects is necessary to identify them for the locationing. Optical sensing is one of the techniques for shape estimations. However, optical techniques cannot work in some situations like smoke in the scene of a fire, or fog, blizzards, dense vegetation, etc. Highly reliable sensing is required especially for rescue robots. Pulse radars utilizing ultra-wide-band (UWB) pulses have an advantage in such situations compared to optical techniques.

Many studies have been done to develop high-resolution algorithms for pulse radar systems [1]–[7]. High-resolution algorithms utilize not only the envelope of the received signal but also the phase of carrier signal. However, it should be noted that the received carrier phase depends on the shape of targets. Especially, $\pi/2$ phase rotation caused by concave is well-known in the field of electric-magnetic wave theory. The effect has not been regarded as a serious problem so far for pulse radar systems, because conventional systems having a narrow bandwidth do not deal with the accuracy. However, in the near future, the problem will become a bottleneck in improving the accuracy of radar systems using UWB pulses. In this paper, we propose an algorithm to compensate the phase rotation caused by the concave and show an application example. The algorithm is presented firstly, which is followed by numerical simulations for validation of the algorithm.

Manuscript received January 21, 2004.
Manuscript revised May 10, 2004.

[†]The authors are with the Department of Communications and Computer Engineering, Graduate School of Informatics, Kyoto University, Kyoto-shi, 606-8501 Japan.
a) E-mail: t-sakamo@aso.cce.i.kyoto-u.ac.jp

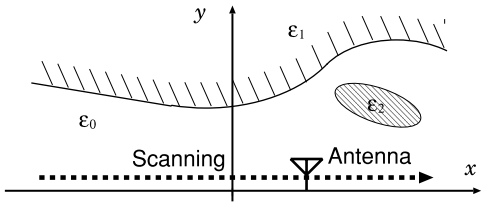

Fig. 1 The coordinates and an example of a target complex permittivity.

2. System Model

We assume a mono-static radar system in this paper. An omni-directional antenna is scanned along a straight line. UWB pulses are transmitted at a fixed interval and received by the antenna. The received data is A/D converted and stored in a memory. We estimate target shapes using the data. Figure 1 shows the system model.

We deal with a 2-dimensional problem, and TE-mode wave. Targets and the antenna are located on a plane. We define r-space as the real space, where targets and the antenna are located. We express r-space with the parameter (x, y). Both x and y are normalized by λ, which is the center wavelength of the transmitted pulse in a vacuum. We assume $y > 0$ for simplicity. The antenna is scanned along x-axis in r-space. We define $s'(X, Y)$ as the received electric field at the antenna location $(x, y) = (X, 0)$, where we define Y with time t and speed of the light c as $Y = ct/(2\lambda)$. We apply a matched filter of transmitted waveform for $s'(X, Y)$. We define $s(X, Y)$ as the output of the filter. We define d-space as the space expressed by (X, Y). We normalize X and Y by λ and the center period of transmitted waveform, respectively. The transform from d-space to r-space corresponds to imaging which we deal with in this paper.

3. Phase Rotation and High-Resolution Imaging

3.1 Phase Rotation and Boundary Shape

In this section, we explain the $\pi/2$ phase rotation caused by concaves. A wave changes its phase after it passes through a caustic [8], [9]. Here, physically singular points are called caustics.

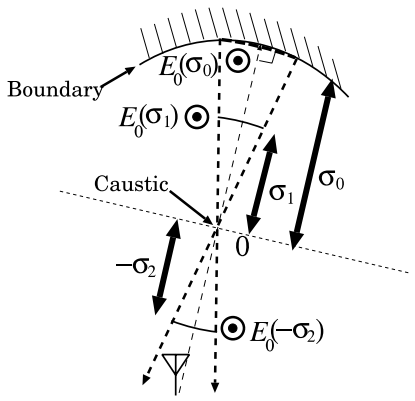

Fig. 2 A concave and phase rotation of signal.

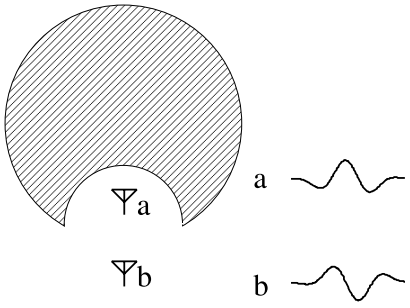

Fig. 3 Phase rotation and antenna position.

First, we introduce geometric optics in order to explain this effect. By using Luneburg-Kline expansion, an electric field can be expressed as

$$E(\boldsymbol{r}) \simeq \mathrm{e}^{-\mathrm{j}k\Phi(\boldsymbol{r})} \sum_{m=0}^{\infty} (-\mathrm{j}k)^{-m} E_m(\boldsymbol{r}), \tag{1}$$

where k is the wave number, $E(\boldsymbol{r})$ is the electric field at the position vector $\boldsymbol{r}$ and $\Phi(\boldsymbol{r})$ is called eikonal. Constant values of the eikonal represent surfaces of constant phase. Therefore, $\nabla\Phi$ represents the direction of the propagation.

The reflected wave comes from the part of target boundary which is orthogonal to $\nabla\Phi$ as in Fig. 2. This means that the electromagnetic wave of constant phase along the target boundary is re-emitted toward the antenna. In the figure, E_0 is the 0-th factor of the reflected electric field in Eq. (1). Therefore, $E_0(\sigma_1)$ in Fig. 2 can be expressed with $E_0(\sigma_0)$ using GO (Geometric Optics) theory as

$$E_0(\sigma_1) = \sqrt{\sigma_0/\sigma_1} E_0(\sigma_0). \tag{2}$$

In the same way, we obtain $E_0(-\sigma_2)$ using GO theory as

$$E_0(-\sigma_2) = \sqrt{-\sigma_0/\sigma_2} E_0(\sigma_0). \tag{3}$$

Note that the inside of the square root in Eq. (3) becomes negative in this case because $\sigma_0, \sigma_2 > 0$ holds. We can interpret the negative value in square root as an imaginary number, which means the phase of $E_0(\sigma_2)$ is advanced compared to $E_0(\sigma_0)$ by $\pi/2$. This explanation helps us to develop a phase compensation algorithm because it is obvious what is the main factor of the phase rotation.

3.2 An Example of Phase Rotation

In this subsection, we show an example of phase rotation explained in the previous subsection. Figure 3 shows a received waveform for each antenna position. Here, the antenna is omni-directional and used as a monostatic radar. The target is a round perfect conductor with a concave at the bottom side. Note that the antenna "a" is inside the concave and the antenna "b" is outside the concave. The received waveform ideally corresponds to an auto-correlation function of the original waveform only if the received signal suffers no phase rotation because the received waveforms are the output of a matched filter. The waveform "a" has a peak at the center because it has not passed through a caustic. On the other hand, the waveform "b" has a peak shifted by $\lambda/4$. We have also confirmed the difference of peak positions between "a" and "b" is precisely $\lambda/4$, which means the phase rotation of $\pi/2$. All we have to do is to detect the waves which passed through caustics and to compensate for the phase rotation.

4. SEABED Algorithm

4.1 Outline of SEABED Algorithm

We propose a phase compensation algorithm in this paper. As an example, we utilize SEABED algorithm because it has an advantage that the detection of caustic is easy compared to other methods. Here, we briefly explain the SEABED algorithm first.

We have already developed a non-parametric shape estimation algorithm based on BST (Boundary Scattering Transform) [10]. We call the algorithm SEABED (Shape Estimation Algorithm based on BST and Extraction of Directly scattered waves). The algorithm utilizes the existence of a reversible transform BST between target shapes and pulse delays. We have clarified that the SEABED has an advantage of direct estimation of target boundaries using inverse transform, which is a mathematically complete solution for the inverse problem. The algorithm has a remarkable performance in estimating target shapes. However, phase rotations of scattered waves caused by concave surfaces cause a great deal of degradation in estimating accuracies. We have proposed an algorithm which simultaneously estimates target locations and scattered waveforms [11], [12]. The algorithm works well, but it is applicable only for point targets. Therefore, it is required to develop a phase compensation algorithm which can estimate the shape of more general targets.

4.2 Boundary Scattering Transform

The SEABED utilizes the existence of a reversible transform between quasi wavefronts and target boundary surfaces. We

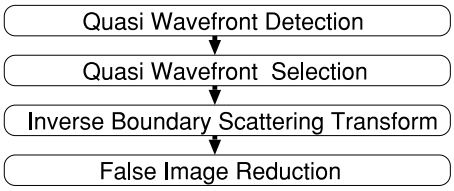

Fig. 4 Outline of the SEABED algorithm.

assume that each target has a uniform complex permittivity, and surrounded by a smooth boundary. We also assume that the propagation speed is known. Here, we assume the medium of direct path is vacuum for simplicity.

Boundary Scattering Transform (BST) is expressed as

$$X = x + y\mathrm{d}y/\mathrm{d}x, \tag{4}$$

$$Y = y\sqrt{1 + (\mathrm{d}y/\mathrm{d}x)^2}, \tag{5}$$

where (X, Y) is a point on a quasi wavefront. (x, y) is a point on target boundary, and we assume $y > 0$ and $Y > 0$ [10]. We have clarified that the inverse transform of BST is given by

$$x = X - Y\mathrm{d}Y/\mathrm{d}X, \tag{6}$$

$$y = Y\sqrt{1 - (\mathrm{d}Y/\mathrm{d}X)^2}, \tag{7}$$

where we assume $|\mathrm{d}Y/\mathrm{d}X| \leq 1$. We call the transform in Eqs. (6) and (7) Inverse Boundary Scattering Transform (IBST).

4.3 SEABED Procedure

First, we extract a quasi wavefront from $s(X, Y)$ in SEABED. Quasi wavefronts have to satisfy the condition $\mathrm{d}s(X, Y)/\mathrm{d}Y = 0$ and $|\mathrm{d}Y/\mathrm{d}X| \leq 1$. The latter condition ensures Y in Eq. (7) to be a real number. Furthermore, we adopt a condition $|s(X_i, Y_i)/s(X_{i+1}, Y_{i+1})| < T_\mathrm{r}$ to prevent an interference, where (X_i, Y_i) and (X_{i+1}, Y_{i+1}) are points on a quasi wavefront and next to each other. This condition is based on that large changes of amplitude in the same quasi wavefront is not rational. We sequentially extract the set of points (X, Y). Next, we select quasi wavefronts with large power and eliminate undesirable components. Finally, we apply IBST to the extracted quasi wavefront and estimate the target shape. Figure 4 shows the outline of the SEABED algorithm.

4.4 An Application Example of SEABED

We show an example of application of SEABED algorithm. Figure 5 shows an example of target boundary surface. The inner domain in the figure is filled with perfect electric conductor, and the outer domain is filled with air. Estimation of this target shape is one of the most difficult cases because it includes convex surfaces, a concave surface and edge points. In most of actual situations, estimation of a target shape is easier than this example.

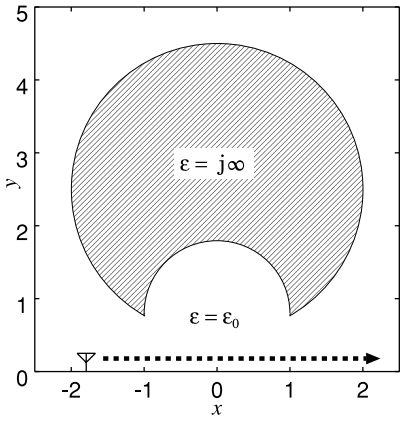

Fig. 5 Target model.

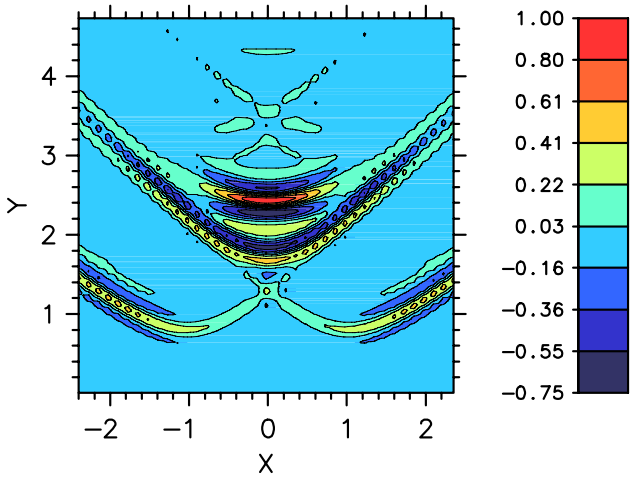

Fig. 6 Observed signal.

Figure 6 shows the received data from the assumed target. We assume $S/N = \infty$ in this section for simplicity. We obtain this signal by utilizing FDTD (Finite Difference Time Domain) method. We receive the signal at the 39 locations whose intervals are 0.125λ. Next, we extract quasi wavefronts using the conditions mentioned in the previous subsection. We adopt an empirically chosen value $T_\mathrm{r} = 1.11$. The extracted quasi wavefronts are shown in Fig. 7. Five quasi wavefronts are extracted in the figure. Finally, we obtain the estimated target boundaries by applying IBST to the extracted wavefronts. Figure 8 shows the estimated target boundary surfaces using the SEABED. The symbols located at the bottom of the figure show the locations of the antenna, where we receive signals. The broken line and the solid lines are the real target boundary surface and the estimated target boundary surfaces, respectively. The estimation accuracy on the concave surface suffers degradation compared to the straight surface. This is caused by the phase rotation occurred at the caustic to the echoes from the concave surface.

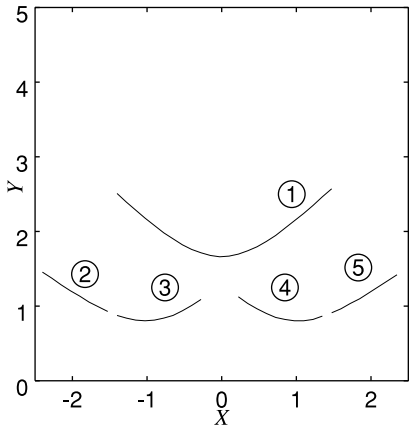

Fig. 7 Extracted quasi wavefronts.

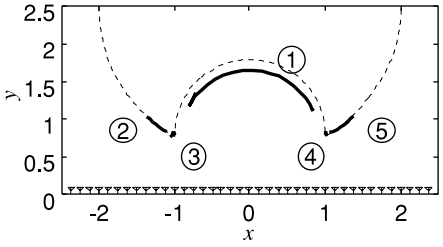

Fig. 8 Estimated target shape using SEABED.

5. Phase Compensation for IBST

5.1 Phase Compensation Algorithm for IBST

In the previous section, we described that the SEABED has an estimation error caused by the phase rotation. The phase rotation depends on the shape of target. It is possible to compensate for the phase rotation if the condition of phase rotation can be expressed using the extracted quasi wavefronts. We define the IBST vector $\boldsymbol{v}_{\mathrm{IBST}}$ as

$$\boldsymbol{v}_{\mathrm{IBST}} = \begin{bmatrix} -Y\mathrm{d}Y/\mathrm{d}X, \\ Y\sqrt{1-(\mathrm{d}Y/\mathrm{d}X)^2} \end{bmatrix}. \tag{8}$$

Equation (6) and Eq. (7) are expressed as

$$\begin{bmatrix} x \\ y \end{bmatrix} - \begin{bmatrix} X \\ 0 \end{bmatrix} = \boldsymbol{v}_{\mathrm{IBST}}. \tag{9}$$

The caustic curve of a target boundary is given as

$$x_{\mathrm{f}} = x - \frac{\mathrm{d}y/\mathrm{d}x}{\mathrm{d}^2y/\mathrm{d}x^2}\left\{(\mathrm{d}y/\mathrm{d}x)^2+1\right\}, \tag{10}$$

$$y_{\mathrm{f}} = y + \frac{1}{\mathrm{d}^2y/\mathrm{d}x^2}\left\{(\mathrm{d}y/\mathrm{d}x)^2+1\right\}. \tag{11}$$

Substituting Eq. (7) for Eq. (5) and solving for $\mathrm{d}y/\mathrm{d}x$, we obtain

$$\mathrm{d}y/\mathrm{d}x = \frac{\mathrm{d}Y/\mathrm{d}X}{\sqrt{1-(\mathrm{d}Y/\mathrm{d}X)^2}}. \tag{12}$$

Table 1 ϕ and the relative location of caustic for the antenna.

ϕ	shape
$-\pi/2$	plane
⋮	inside of concave
0	on caustic of concave
⋮	outside of concave
$\pi/4$	point target
⋮	convex
$\pi/2$	plane

Similarly, we obtain $\mathrm{d}^2y/\mathrm{d}x^2$ as

$$\frac{\mathrm{d}^2y}{\mathrm{d}x^2} = \frac{\dfrac{\mathrm{d}^2Y}{\mathrm{d}X^2}}{\left\{1-\left(\frac{\mathrm{d}Y}{\mathrm{d}X}\right)^2\right\}^{3/2}\left\{1-\left(\frac{\mathrm{d}Y}{\mathrm{d}X}\right)^2 - Y\frac{\mathrm{d}^2Y}{\mathrm{d}X^2}\right\}}. \tag{13}$$

It is remarkable that the 1st- and 2nd-order derivatives of the target boundary is expressed using the quasi wavefront and its 1st- and 2nd-order derivatives. It is thus possible to express the right-hand side of Eq. (10) and Eq. (11) using the quasi wavefront and its 1st- and 2nd-order derivatives. We obtain

$$\begin{bmatrix} x_{\mathrm{f}} \\ y_{\mathrm{f}} \end{bmatrix} - \begin{bmatrix} X \\ 0 \end{bmatrix} = \tan\phi\boldsymbol{v}_{\mathrm{IBST}}, \tag{14}$$

where ϕ is defined as

$$\phi = \tan^{-1}\left\{\frac{1-(\mathrm{d}Y/\mathrm{d}X)^2}{Y\mathrm{d}^2Y/\mathrm{d}X^2}\right\}. \tag{15}$$

We see that a caustic is on the line which connects the antenna and the boundary. ϕ is the parameter which shows the relative position of the caustic for the antenna. As we mentioned in the previous section, we observe the phase rotation of $\pi/2$ in received signals if the antenna is located in the outer part of caustic for a concave boundary. This condition can be expressed using the quasi wavefront as

$$0 < \phi < \pi/4. \tag{16}$$

The relationship between ϕ and target shapes is shown in Table 1. Figure 9 illustrates the angle ϕ and the target shape. Figure 10 explains the meaning of ϕ using $\boldsymbol{v}_{\mathrm{IBST}}$ and $\boldsymbol{v}_{\mathrm{c}}$, where we define $\boldsymbol{v}_{\mathrm{c}} = [x_{\mathrm{f}}, y_{\mathrm{f}}]^{\mathrm{T}} - [X, 0]^{\mathrm{T}}$.

In order to compensate for the phase rotation, we modify IBST as

$$x = X - \{Y + f(\phi)\}\,\mathrm{d}Y/\mathrm{d}X, \tag{17}$$

$$y = \{Y + f(\phi)\}\sqrt{1-(\mathrm{d}Y/\mathrm{d}X)^2}, \tag{18}$$

where $f(\phi)$ is defined as

$$f(\phi) = \begin{cases} 1/8 & (0 < \phi < \pi/4) \\ 0 & (\text{otherwise}). \end{cases} \tag{19}$$

Note that the compensation of $\lambda/8$ is required because the phase rotation $\lambda/4$ corresponds to a round-trip delay. We can directly detect a caustic and antenna position with quasi wavefronts utilizing ϕ.

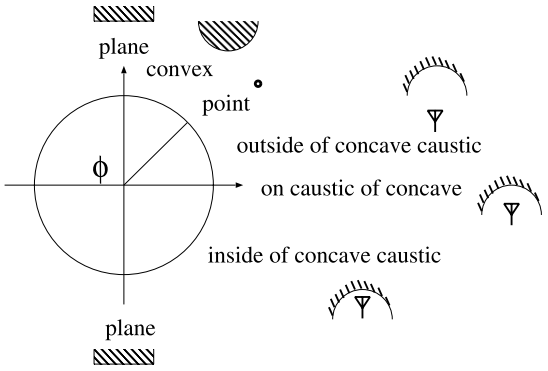

Fig. 9 ϕ and boundary shape.

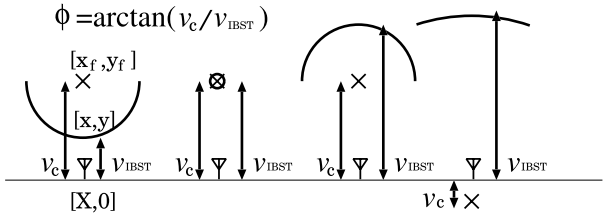

Fig. 10 Locations of antenna, caustic and target.

6. An Application Example of the Phase Compensation Algorithm

In this section, we show an application example of the phase compensation algorithm. We assume $S/N = \infty$ in this section for simplicity. Figure 11 shows a calculated ϕ for each quasi wavefront. The calculated ϕ is plotted with X in the figure. Calculated ϕ are located in the correct region for quasi wavefronts "2" and "5." On the other hand, edge diffraction "3" and "4" have ϕ around $\pi/4$, which means it is close to a point target. As for quasi wavefront "1," calculated ϕ is about $\pi/8$ at the center, but the both ends has wrong ϕ in the convex region.

We show an application example of the modified IBST using the calculated ϕ above. Figure 12 shows the estimated target shapes using the modified IBST. Most of the errors at the caustic in Fig. 8 are improved in this case. However, the both ends of "1" still have error because they are regarded as convex by the algorithm. Furthermore, the estimation of edge points have error in this case because part of them are regarded as concave and undesirable phase compensation was made.

In order to prevent the problems of phase compensation, we propose another algorithm for phase compensation. First, we calculate the average ϕ for each quasi wavefront. Next, we determine phase compensation using the averaged ϕ. We set margin for the threshold to make the algorithm stable. We adopt empirically chosen condition $5^\circ < \phi < 40^\circ$ for phase compensation. Averaged ϕ for each quasi wavefront is shown in Table 2. Figure 13 shows the estimated target shape using averaged ϕ. We see the estimation accuracy is improved without sacrificing the resolution.

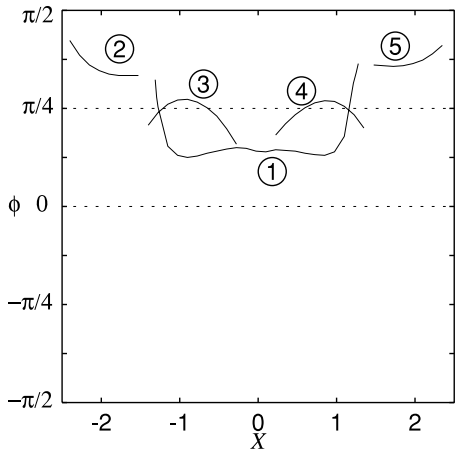

Fig. 11 ϕ for each quasi wavefront.

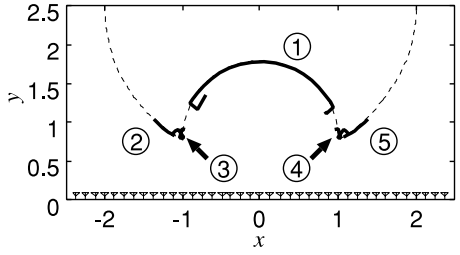

Fig. 12 Phase compensated estimation.

Table 2 Average ϕ and shape determination.

Quasi wavefront	ϕ [degree]	Estimated shape
#1	28.1	concave
#2	64.3	convex
#3	42.4	concave
#4	42.7	concave
#5	66.9	convex

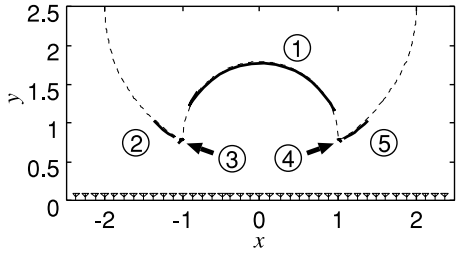

Fig. 13 Estimation with a margin of decision for ϕ.

7. Limitation of the Proposed Algorithm

In this section, we explain the limitation of the proposed algorithm. First, we investigate the performance of the proposed algorithm in a noisy environment. Figure 14 shows the simulation result of the shape estimation for S/N=20 dB. The proposed algorithm works well to some extent in this case even with noise. However, one of the edge points

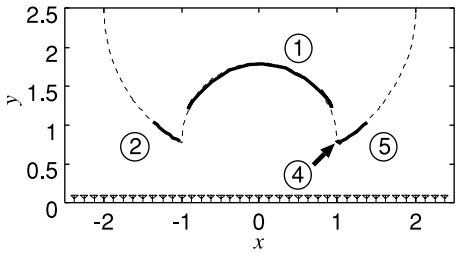

Fig. 14 Estimated target shape for S/N=20 dB.

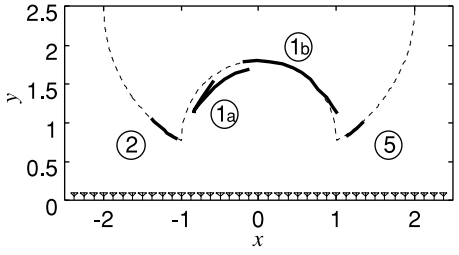

Fig. 15 Estimated target shape for S/N=10 dB.

("3" in Fig. 13) is not estimated because the power of the diffracted wave is smaller than that of the reflected waves. Figure 15 shows the simulation result of the shape estimation for S/N=10 dB. In this figure, we see that the concave surface ("1" in Fig. 13) is erroneously divided into two parts ("1_a" and "1_b" in Fig. 15) in the extraction procedure of quasi wavefronts in SEABED algorithm. Furthermore, the phase compensation algorithm does not works for one of them although it works properly for the other. This is because the phase compensation algorithm requires the 2nd-order derivatives of quasi wavefronts, which can be unstable in noisy situation. Additionally, neither of the edge points are detected because of the same reason as in the case of 20 dB. This result shows that the proposed algorithm requires a relatively high S/N, which is usually satisfied for the indoor applications considered in this paper. The estimation accuracy degrades for low S/N although the averaging procedure of ϕ contribute to the stability of the algorithm to some extent. Further studies are required to make this algorithm applicable to situations with low S/N such as GPR (Ground Penetrating Radar) systems.

We have shown an application example of the proposed algorithm only for a target in Fig. 5. However, we have confirmed that the proposed algorithm is applicable for targets with any size of concave or convex structures as far as the reflected waves from such structures can be identified in the received signals. In addition, it is also applicable for an edge point because SEABED can deal with a diffraction wave. However, it is difficult to apply the proposed algorithm to targets which cause severe interference. This is because the proposed algorithm needs directly scattered wave including a reflection wave and diffraction wave from the target.

8. Conclusion

High-resolution shape estimation algorithms utilize the information of carrier phase. The estimation accuracy degrades on a certain condition because the carrier phase depends on the target shape. We proposed a phase compensation algorithm for SEABED algorithm. SEABED is a non-parametric algorithm of estimating target shapes for pulse radar systems. SEABED first extracts quasi wavefronts, which is suitable for phase compensation. We have clarified that phase compensation can be possible using a value ϕ which is calculated using a quasi wavefront and its 1st- and 2nd-order derivatives. We have modified IBST to compensate for phase rotation using ϕ. The modified IBST has a problem of instability of ϕ. We should note that ϕ suffers instability of 2nd-order derivative. We also modified the phase compensation algorithm to improve stability using averaged ϕ. The proposed phase compensation algorithm works well and estimated target surface accurately including its edge points.

Acknowledgment

We thank Dr. Masahiko Nishimoto at the Department of Electrical and Computer Engineering, Kumamoto University, Japan for his precious advice. This work is supported in part by the 21st Century COE Program (Grant No. 14213201).

References

[1] D. Nahamoo, S.X. Pan, and A.C. Kak, "Synthetic aparture diffraction tomography and its interpolation-free computer implementation," IEEE Trans. Sonics Ultrason., vol.31, no.4, pp.218–229, 1984.
[2] M.B. Dobrin and C.H. Savit, Introduction to Geophysical Prospecting, Fourth Edition, McGraw-Hill, New York, 1988.
[3] J.V. Candy and C. Pichot, "Active microwave imaging: A model-based approach," IEEE Trans. Antennas Propag., vol.39, no.3, pp.285–290, 1991.
[4] P. Chaturvedi and R.G. Plumb, "Electromagnetic imaging of underground targets using constrained optimization," IEEE Trans. Geosci. Remote Sens., vol.33, no.3, pp.551–561, 1995.
[5] T. Sato, K. Takeda, T. Nagamatsu, T. Wakayama, I. Kimura, and T. Shinbo, "Automatic signal processing of front monitor radar for tunnelling machines," IEEE Trans. Geosci. Remote Sens., vol.35, no.2, pp.354–359, 1997.
[6] T. Sato, T. Wakayama, and K. Takemura, "An imaging algorithm of objects embedded in a lossy dispersive medium for subsurface radar data processing," IEEE Trans. Geosci. Remote Sens., vol.38, no.1, pp.296–303, 2000.
[7] T. Takenaka, H. Jia, and T. Tanaka, "Microwave imaging of an anisotropic cylindrical object by a forward-backward time-stepping method," IEICE Trans. Electron., vol.E84-C, no.12, pp.1910–1916, Dec. 2001.
[8] G.L. James, Geometrical Theory of Diffraction for Electromagnetic Waves, IEE Electromagnetic Waves Series 1, Peter Peregrinus Ltd., UK, 1980.
[9] D.A. McNamara, C.W.I. Pistorius, and J.A.G. Malherbe, Introduction to the Uniform Geometrical Theory of Diffraction, Artech House, Boston, 1990.

[10] T. Sakamoto and T. Sato, "A target shape estimation algorithm for UWB pulse radar systems based on boundary scattering transform," IEICE Trans. Commun., vol.E87-B, no.5, pp.1357–1365, May 2004.
[11] T. Sakamoto and T. Sato, "An estimation method of target location and scattered waveforms for UWB pulse radar systems," Proc. 2003 IEEE International Geoscience and Remote Sensing Symposium, pp.4013–4015, Toulouse, France, 2003.
[12] T. Sakamoto and T. Sato, "An estimation method of target location and scattered waveforms for UWB pulse radar systems," IEICE Trans. Commun., vol.E87-B, no.6, pp.1631–1638, June 2004.

Appendix A: Derivation of Eqs. (2) and (3)

We show the derivation of Eqs. (2) and (3) based on the reference papers [8], [9]. Helmholtz equation is given as

$$\nabla^2 \boldsymbol{E} + k^2 \boldsymbol{E} = 0. \tag{A·1}$$

Equation (1) can be expressed as

$$\boldsymbol{E}(\boldsymbol{r}) \simeq \mathrm{e}^{-\mathrm{j}k\Phi(\boldsymbol{r})} \sum_{m=0}^{\infty} (-\mathrm{j}k)^{-m} \boldsymbol{E}_m(\boldsymbol{r}) \tag{A·2}$$

using the vector $\boldsymbol{E}(\boldsymbol{r})$ of electric field. Substituting the asymptotic expression Eq. (A·2) into Eq. (A·1), we obtain the 0-th order transport equation as

$$(\nabla\Phi \cdot \nabla)\boldsymbol{E}_0 + \frac{1}{2}(\nabla^2\Phi)\boldsymbol{E}_0 = 0. \tag{A·3}$$

The general solution of Eq. (A·3) is

$$\boldsymbol{E}_0(\sigma) = \boldsymbol{E}_0(\sigma_0)\mathrm{e}^{-\frac{1}{2}\int_{\sigma_0}^{\sigma} \nabla^2\Phi \mathrm{d}\sigma}, \tag{A·4}$$

where σ is the length along a lay path. $\nabla^2\Phi$ is expressed as

$$\nabla^2\Phi = \frac{1}{\sigma} \tag{A·5}$$

with σ in the coordinates in Fig. 2. Finally, substituting Eq. (A·5) into Eq. (A·4), we obtain

$$\boldsymbol{E}_0(\sigma) = \boldsymbol{E}_0(\sigma_0)\sqrt{\sigma_0/\sigma}. \tag{A·6}$$

Equation (A·6) can easily lead to Eqs. (2) and (3). Here, we should note that 2-dimensional TE-mode wave has only one component which can be expressed using a scalar variable.

Appendix B: Derivation of Eqs. (10) and (11)

We show the derivation of Eqs. (10) and (11) in this section. First, let us define $\boldsymbol{v}_\mathrm{f}$ as

$$\boldsymbol{v}_\mathrm{f} = \begin{bmatrix} x_\mathrm{f} \\ y_\mathrm{f} \end{bmatrix} - \begin{bmatrix} x \\ y \end{bmatrix}. \tag{A·7}$$

$\boldsymbol{v}_\mathrm{f}$ should satisfy the conditions such as

$$|\boldsymbol{v}_\mathrm{f}| = r_\mathrm{c}, \text{and} \tag{A·8}$$

$$\boldsymbol{v}_\mathrm{f} \parallel \boldsymbol{v}_\mathrm{n}, \tag{A·9}$$

where r_c and $\boldsymbol{v}_\mathrm{n}$ are the radius of curvature and the normal vector of a target boundary surface, respectively. The radius of curvature of a target boundary surface is given as

$$r_\mathrm{c} = \frac{\left\{1 + (\mathrm{d}y/\mathrm{d}x)^2\right\}^{3/2}}{\left|\mathrm{d}^2y/\mathrm{d}x^2\right|}. \tag{A·10}$$

The normal vector of a target boundary surface is given as

$$\boldsymbol{v}_\mathrm{n} = \frac{\mathrm{d}^2y/\mathrm{d}x^2}{\left|\mathrm{d}^2y/\mathrm{d}x^2\right|\sqrt{1 + (\mathrm{d}y/\mathrm{d}x)^2}} \begin{bmatrix} -\mathrm{d}y/\mathrm{d}x \\ 1 \end{bmatrix}. \tag{A·11}$$

Therefore, we can conclude that $\boldsymbol{v}_\mathrm{f}$ can be expressed as

$$\boldsymbol{v}_\mathrm{f} = \frac{1 + (\mathrm{d}y/\mathrm{d}x)^2}{\mathrm{d}^2y/\mathrm{d}x^2} \begin{bmatrix} -\mathrm{d}y/\mathrm{d}x \\ 1 \end{bmatrix}. \tag{A·12}$$

Finally, the caustic curve $[x_\mathrm{f}, y_\mathrm{f}]$ is expressed as in Eqs. (10) and (11).

Appendix C: Derivation of Eq. (13)

Differentiating the both sides of Eq. (12) with regard to x, we obtain

$$\frac{\mathrm{d}^2y}{\mathrm{d}x^2} = \frac{\dfrac{\mathrm{d}^2Y}{\mathrm{d}X^2}}{\left\{1 - \left(\dfrac{\mathrm{d}Y}{\mathrm{d}X}\right)^2\right\}^{3/2}} \frac{\mathrm{d}X}{\mathrm{d}x}. \tag{A·13}$$

In order to obtain $\mathrm{d}X/\mathrm{d}x$ in the right hand side of Eq. (A·13), we have to differentiate the both sides of Eq. (4) with regard to x. We utilize a chain rule to get a derivative as

$$\frac{\mathrm{d}X}{\mathrm{d}x} = \frac{\partial X}{\partial x} + \frac{\partial X}{\partial y}\frac{\mathrm{d}y}{\mathrm{d}x} + \frac{\partial X}{\partial(\mathrm{d}y/\mathrm{d}x)}\frac{\mathrm{d}^2y}{\mathrm{d}x^2}. \tag{A·14}$$

Substituting Eq. (4) into Eq. (A·14), we obtain

$$\mathrm{d}X/\mathrm{d}x = 1 + (\mathrm{d}y/\mathrm{d}x)^2 + y\mathrm{d}^2y/\mathrm{d}x^2. \tag{A·15}$$

Next, substituting Eq. (A·15) into Eq. (A·13), we obtain

$$\frac{\mathrm{d}^2y}{\mathrm{d}x^2} = \frac{\mathrm{d}^2Y}{\mathrm{d}X^2} \frac{\left\{1 + (\frac{\mathrm{d}y}{\mathrm{d}x})^2 + y\frac{\mathrm{d}^2y}{\mathrm{d}x^2}\right\}}{\left\{1 - \left(\frac{\mathrm{d}Y}{\mathrm{d}X}\right)^2\right\}^{3/2}}. \tag{A·16}$$

Solving Eq. (A·16) for $\mathrm{d}^2y/\mathrm{d}x^2$, we obtain

$$\frac{\mathrm{d}^2y}{\mathrm{d}x^2} = \frac{\frac{\mathrm{d}^2Y}{\mathrm{d}X^2}\left\{1 + (\frac{\mathrm{d}y}{\mathrm{d}x})^2\right\}}{\left\{1 - \left(\frac{\mathrm{d}Y}{\mathrm{d}X}\right)^2\right\}^{3/2} - y\frac{\mathrm{d}^2Y}{\mathrm{d}X^2}}. \tag{A·17}$$

Finally, substituting Eqs. (7) and (12) into Eq. (A·17), we obtain Eq. (13).

Takuya Sakamoto received the B.E. degree from Kyoto University in 2000, the M.I. degree from Graduate School of Informatics, Kyoto University in 2002. He is currently studying for the Ph.D. degree at Graduate School of Informatics, Kyoto University. His current research interest is in digital signal processing. He is a member of the IEEJ and the IEEE.

Toru Sato received his B.E., M.E., and Ph.D. degrees in electrical engineering from Kyoto University, Kyoto, Japan in 1976, 1978, and 1982, respectively. He has been with Kyoto University since 1983 and is currently a Professor in the Department of Communications and Computer Engineering, Graduate School of Informatics. His major research interests have been system design and signal processing aspects of atmospheric radars, radar remote sensing of the atmosphere, observations of precipitation using radar and satellite signals, radar observation of space debris, and signal processing for subsurface radar signals. Dr. Sato was awarded Tanakadate Prize in 1986. He is a member of the Society of Geomagnetism and Earth, Planetary and Space Sciences, the Japan Society for Aeronautical and Space Sciences, the Institute of Electrical and Electronics Engineers, and the American Meteorological Society.